Modeling and experimental validation of the solar loop for absorption solar cooling system using double glazed collectors

Olivier Marc Marc, Jean-Philippe Praene, Alain Bastide, Franck Lucas

Accepted Manuscript

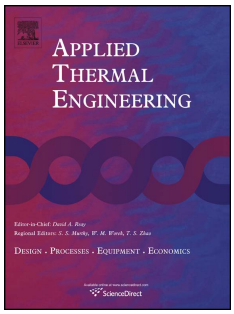

Title: Modeling and experimental validation of the solar loop for absorption solar cooling system using double glazed collectors

Authors: Olivier Marc, Jean-Philippe Praene, Alain Bastide, Franck Lucas

PII: S1359-4311(10)00393-5

DOI: 10.1016/j.applthermaleng.2010.09.006

Reference: ATE 3233

To appear in: *Applied Thermal Engineering*

Received Date: 24 June 2010

Revised Date: 23 August 2010

Accepted Date: 4 September 2010

Please cite this article as: O. Marc, J.-P. Praene, A. Bastide, F. Lucas. Modeling and experimental validation of the solar loop for absorption solar cooling system using double glazed collectors, Applied Thermal Engineering (2010), doi: 10.1016/j.applthermaleng.2010.09.006

Modeling and experimental validation of the solar loop for absorption solar cooling system using double glazed collectors

Olivier Marc*, Jean-Philippe Praene, Alain Bastide, Franck LucasLaboratory of Physical and Mathematical Engineering for Energy and Environment (PIMENT)University of La Reunion, FranceCorresponding author: olivier.marc@univ-reunion.fr

Abstract Solar cooling applied to buildings is without a doubt an interesting alternative for reducing energy consumption in traditional mechanical steam compression air conditioning systems. The study of these systems should have a closely purely fundamental approach including the development of numerical models in order to predict the overall installation performance. The final objective is to estimate cooling capacity, power consumption, and overall installation performance with relation to outside factors (solar irradiation, outside temperature...). The first stage in this work consists of estimating the primary energy produced by the solar collector field. The estimation of this primary energy is crucial to ensure the evaluation of the cooling capacity and therefore the cooling distribution and thermal comfort in the building. Indeed, the absorption chiller performance is directly related to its heat source. This study presents dynamic models for double glazing solar collectors and compares the results of the simulation with experimental results taken from our test bench (two collectors). In the second part, we present an extensive collector field model (36 collectors) from our solar cooling installation at The University Institute of Technology in St Pierre, Reunion Island as well as our stratified tank storage model. A comparison of the simulation results with real scale solar experimental data taken from our installation enables validation of the double glazing solar collector and stratified tank dynamic models.

Key words: Solar cooling; Double glazed solar collector; Absorption; Storage tank; Simulation; Experimental set up; Tropical climate.

1. Introduction In summer, particularly under tropical climate, air conditioning has the highest energy expenditure in buildings. Solar cooling applied in buildings is without a doubt an interesting alternative for solving problems of electrical over-consumption in traditional compression vapor air conditioning. Solar energy use in cooling buildings offers the advantage of using an inexhaustible and free heat source which caters for cooling needs most of the time [1]. The study of these systems should be close to experimental pilot installations to investigate the appropriate design [2] and to evaluate the overall performance both in different building types and climates [3, 4]. But it's not the only way, a purely fundamental approach including development of numerical models can be carried out [5-6] that enable the prediction of the overall installation performance. The final objective of this model is to estimate the cooling capacity, power consumption, and overall installation performance according to operating conditions (solar irradiation, outside temperature, occupancy...). As these parameters are highly variable from one moment to another, modeling should imperatively consider system dynamics to be able to integrate all the physical phenomena the most accurately as possible.

The principle diagram of a solar cooling installation is presented in Fig. 1. The heat generated by the thermal solar collector field (1) is stored in the hot water tank (2) before feeding the absorption chiller generator (3). Cold water produced by the absorption chiller evaporator is stored in the cold water tank (4) before feeding fan coils in the building to be cooled (6). Finally, the absorber and the condenser of the absorption chiller are cooled by the cooling tower.

Fig. 1: Diagram of a solar cooling installation: 1. Solar collector field, 2. Hot water tank, 3. Absorption chiller, 4. Cold water tank 5. Cooling tower 6. Building

The first step in modeling a solar cooling installation is to estimate the primary energy produced by the thermal solar collector field. This primary energy is stored in a hot water tank before feeding the absorption chiller generator. The estimation of this primary energy is crucial to ensure the proper evaluation of the cooling capacity and thus the thermal comfort inside the buildings. Indeed, the absorption chiller performance is directly related to the quality of the heat source [7]. There are currently three main solar collector technologies suitable for solar cooling installations using single effect absorption chillers: the vacuum tube collectors, the single glazed flat plate collectors and the double glazed flat plate collectors. The single effect absorption chillers are the most common and do not require temperatures at the inlet of the generator above 100°C. Vacuum tube collectors and flat plate single glazing collectors are the most widespread technologies and many models can be found in the literature [8,9, 10, 11, 12, 13]. Evacuated tubes collectors remain expensive and their efficiency depends on the sealing between the glazed tube and the duct, the vacuum no longer exists after several years and thus the convective heat loss becomes significant. The single glazed flat plate collectors are indeed much cheaper but they are less efficient when used to produce water above 70°C. We chose to study double glazed flat plate collectors which are much less expensive than vacuum tube technology and more efficient than conventional single-glazed flat plate collectors. Double glazing minimizes heat loss from the upper collector surface and therefore reinforces the greenhouse effect occurring inside the collector. In this work, we present the dynamics model for a solar double glazing collector and compare simulation results with experimental data obtained from our test bench (2 collectors). In the second part, we put forward an extended model of the whole solar loop at our solar cooling installation at The University Institute of technology in St Pierre, Reunion Island. This model takes the collector field (90 m²) as well as the stratified storage tank into consideration. A comparison between simulation results and data from the full scale experimental solar cooling facility validates the dynamic models of the solar loop and stratified tank.

2. Installation Modeling *2.1. Design of the double glazed flat plate collector*The double glazed flat plate collector under study is composed of seven layers as seen in Fig. 2. The upper collector is composed of two glass layers (1,3) separated by an air gap. The absorbing collector inner surface (5) and the second glazing (3) are separated by a second air layer (4). The transfer fluid (6) runs under the absorbent surface (5). Finally an insulator and support (7) is fixed under the absorber to reduce heat loss.

Fig. 2: Representation of the double glazed collector: 1. First glass layer 2. First air layer 3. Second glass layer 4. Second air layer 5. Absorbent surface 6. Transfer fluid 7. Insulation and support.

The different heat transfer modes involved, can be observed in Fig 2. The first layer of glass (1) is subject to two convection transfers: the first one between the air and the upper side and the second between the first air layer (2) and its underside. It is also subject to two radiative transfers: the first between the sky and its upper side and the second between the underside of the second layer of glass (3). Similarly the second layer of glass (3) is subject to two convection transfers (one between the first layer of air (2) and its upper side and the other between the second layer of air (4) and its underside) and in addition to these two radiative transfers (one with its top surface and the underside of the first layer of glass (1) and the other between the upper surface of the absorber (5) and its bottom surface). The absorbent surface (5) is subjected to two convection transfers (one between the second air layer and its upper side and the other between the transfer fluid (6) and its underside), and in addition to the radiative transfer, between the upper side and the second layer of air (3). The transfer fluid (water) (6) is subject to two convection transfers: the first with the absorber and the second with the isolator. Heat loss from the underside of the collector is characterized by a conductive flux through the isolator and convective exchange between the isolator and the ambient air. Similarly we may note that each layer (1-6) has an additional side wall loss characterized by a conductive flux associated with a convective flux.

*2.2. Double glazed solar collector model*Now that all the heat transfers inside our double glazed solar collector representation have been identified, the energy balances can be expressed as follows :Equation for the first layer of glass (1):

$$M_{g1} \cdot C_{g1} \cdot \frac{dT_{g1}}{dt} = h_{r,g1-sky} \cdot S_{g1} \cdot (T_{sky} - T_{g1}) + h_{r,g1-g2} \cdot S_{g2} \cdot (T_{g2} - T_{g1}) + h_{cv,out} \cdot S_{g1} \cdot (T_{amb} - T_{g1}) + h_{cv,g1-a1} \cdot S_{g1} \cdot (T_{a1} - T_{g1}) + U_{loss} \cdot S_{lat,g1} \cdot (T_{amb} - T_{g1}) \quad (1)$$

Equation for the first air layer (2):

$$\rho_{a1} \cdot V_{a1} \cdot C_{a1} \cdot \frac{dT_{a1}}{dt} = h_{cv,g1-a1} \cdot S_{g1} \cdot (T_{g1} - T_{a1}) + h_{cv,g2-a1} \cdot S_{g2} \cdot (T_{g2} - T_{a1}) + U_{loss} \cdot S_{lat,a1} \cdot (T_{amb} - T_{a1}) \quad (2)$$

Equation for the second glass layer (3):

$$M_{g2} \cdot C_{g2} \cdot \frac{dT_{g2}}{dt} = h_{r,g1-g2} \cdot S_{g2} \cdot (T_{g1} - T_{g2}) + h_{r,g2-abs} \cdot S_{g2} \cdot (T_{abs} - T_{g2})$$

$$+h_{cv,g2-a1} \cdot S_{g2} \cdot (T_{a1} - T_{g2}) + h_{cv,g2-a2} \cdot S_{g2} \cdot (T_{a2} - T_{g2}) + U_{loss} \cdot S_{lat,g2} \cdot (T_{amb} - T_{g2}) \quad (3)$$

Equation for the second air layer (4):

$$\rho_{a2} \cdot V_{a2} \cdot C_{a2} \cdot \frac{dT_{a2}}{dt} = S_{g2} \cdot h_{cv,g2-a2} \cdot (T_{g2} - T_{a2}) + S_{abs} \cdot h_{cv,abs-a2} \cdot (T_{abs} - T_{a2}) + U_{loss} \cdot S_{lat,a2} \cdot (T_{amb} - T_{a2}) \quad (4)$$

Equation for the absorber (5):

$$M_{abs} \cdot C_{abs} \cdot \frac{dT_{abs}}{dt} = h_{r,g2-abs} \cdot S_{abs} \cdot (T_{g2} - T_{abs}) + G \cdot \tau \cdot \alpha \cdot S_{abs} + S_{ech_f} \cdot h_{cv,abs-f} \cdot (T_f - T_{abs}) + h_{cv,abs-a2} \cdot S_{abs} \cdot (T_{a2} - T_{abs}) + U_{loss} \cdot (S_{abs} - S_{ech_f}) \cdot (T_{amb} - T_{abs}) \quad (5)$$

Equation for the transfer fluid (6):

$$m_f \cdot C_f \cdot \left(\frac{\partial T_f}{\partial t} + u \cdot \frac{\partial T_f}{\partial x}\right) = h_{cv,abs-f} \cdot S_{ech_f} \cdot (T_{abs} - T_f) + U_{f-loss} \cdot S_{ech-f} \cdot (T_{amb} - T_f) \quad (6)$$

The following assumptions are made:

- The thermo-physical properties of different materials are independent of temperature.
- The glass surfaces are clean and transparent to solar radiation.
- The conduction transfers inside glass and air layers are disregarded.
- The absorption and transmission coefficients are considered constant and provided by the manufacturer.
- The reflected radiation of the absorber exits the collector.
- Radiation losses from the sides and bottom of the collector are neglected.

2.3. Convection exchange coefficients of the collector

The convection exchange coefficient between the upper surface of the collector and the ambient air depends mainly on wind speed and can be evaluated using the empirical equation proposed by Agarwal and Larson [14]:

$$h_{cv,out} = 3.9 \cdot u_{wind} + 5.62 \quad (7)$$

Where u_{wind} is the wind speed near the collector in $m.s^{-1}$.

The convection heat exchange coefficient between the two layers of glass (g_1 and g_2) is determined thanks to the equations proposed by Duffie and Beckman [15] on natural convection between two flat plates:

$$h_{cv,g1-a1} = h_{cv,g2-a1} = \frac{Nu \cdot \Lambda_{a1}}{e_{a1}} \quad (8)$$

where Λ_{a1} and e_{a1} are respectively the thermal conductivity and thickness of the air between the two layers of glass. The Nusselt number (Nu) is given in the following equation:

$$Nu = \left[0.06 - 0.017\left(\frac{\beta}{90}\right)\right] \cdot Gr^{\frac{1}{3}} \quad (9)$$

where β is the inclined angle of the collector in degrees. The Prandtl number is included in the equation above and is independent of the temperature (Pr = 0.7) [15]. The Grashoff number is given in the following equation:

$$Gr = \frac{g \cdot |T_{g1} - T_{g2}| \cdot e_{a1}^3}{\upsilon^2 \cdot T_{a1}} \quad (10)$$

where T_{g1}, T_{g2} and T_{a1} are the temperatures, of the two glazed layers (g_1 and g_2) and (a_1) in the air cavity, υ is the kinematic viscosity of the air and (g) the gravity. Indices are adjusted in Eq. 8 to determine the convection exchange coefficients between the 2° glass layer and absorber.

$$h_{cv,g2-a2} = h_{cv,abs-a2} = \frac{Nu \cdot \Lambda_{a2}}{e_{a2}} \quad (11)$$

The Nusselt number is calculated in equation (9) and the Grashoff number is:

$$Gr = \frac{g \cdot |T_{g2} - T_{abs}| \cdot e_{a2}^3}{\upsilon^2 \cdot T_{a2}} \quad (12)$$

The following equation proposed by Incropera et al. [16] is used to calculate the convection exchange coefficient between the water transfer fluid and the inner absorber wall:

$$Nu = 0.023 \cdot Re_D^{\frac{4}{5}} \cdot Pr^{0.4} \quad (13)$$

where Pr and Re_D are the Prandtl and Reynolds numbers.The exchange coefficient is obtained in the following equation:

$$h_{cv,abs-f} = h_{cv,ins-f} = \frac{Nu \cdot \Lambda_f}{D_{int_{ech_f}}} \quad (14)$$

Note that all the thermo-physical properties of the fluids are dependent on the temperature of the fluid (T_f).Finally the last two global exchange coefficients are determined in the standard way:

$$U_{loss} = \frac{1}{k_{ins} + \frac{1}{h_{cv,ins-amb}}} \; avec \; k_{ins} = \frac{e_{ins}}{\Lambda_{ins}} \quad (15)$$

$$U_{f-loss} = \frac{1}{\frac{1}{h_{cv,ins-f}} + k_{ins} + \frac{1}{h_{cv,ins-amb}}} \quad (16)$$

2.4. Radiation transfer coefficientsThe radiation exchange coefficient between the upper wall of the collector and the sky is determined in the following equation [15]:

$$h_{r,g1-sky} = \varepsilon_{g1} \cdot \sigma \cdot \left(T_{g1}^2 + T_{sky}^2\right) \cdot \left(T_{g1} + T_{sky}\right) \quad (17)$$

where ε_{g1}, σ, T_{sky} and T_{g1} are the emissivity of glass N°1, the Stefan-Boltzmann constant, the sky temperature and the temperature of glass N°1.The radiation exchange coefficient between the two layers of glass is given in the following equation:

$$h_{r,g1-g2} = \frac{\sigma \cdot \left(T_{g1}^2 + T_{g2}^2\right) \cdot \left(T_{g1} + T_{g2}\right)}{\varepsilon_{g1}^{-1} + \varepsilon_{g2}^{-1} - 1} \quad (18)$$

where ε_{g2} and T_{g2} are the emissivity and temperature of glass N°2.Finally, the radiation exchange coefficient between the second layer of glass and the absorbent surface is given in the following equation:

$$h_{r,g2-abs} = \frac{\sigma \cdot \left(T_{g2}^2 + T_{abs}^2\right) \cdot \left(T_{g2} + T_{abs}\right)}{\varepsilon_{g2}{}^{-1} + \varepsilon_{abs}{}^{-1} - 1} \quad (19)$$

2.5. Stratified tank model

As seen in Fig. 1, the nodes were discretized, nominalization [8, 17] takes the thermal stratification in the hot water storage tank into account. The following equations are related to the first node (1), the intermediate nodes (i) and the last node (n).

$$\rho_1 . V_1 . C_f . \frac{dT_1}{dt} = m_1 . C_f . (T_{i1} - T_1) + \frac{\lambda . S_i}{e_{1,2}} (T_2 - T_1) + m_2 . C_f . (T_2 - T_1) + S_1 . U_1 . (T_a - T_1) \quad (20)$$

$$\rho_i . V_i . C_f . \frac{dT_i}{dt} = m_1 . C_f . (T_{i-1} - T_i) + \frac{\lambda . S_i}{e_i} (T_{i-1} - T_i) + m_2 . C_f . (T_{i+1} - T_i)$$
$$+ S_i . U_i . (T_a - T_i) - \frac{\lambda . S_i}{e_i} (T_i - T_{i+1}) \quad (21)$$

$$\rho_n . V_n . C_f . \frac{dT_n}{dt} = m_1 . C_f . (T_{n-1} - T_n) + \frac{\lambda . S_i}{e_{n-1,n}} (T_{n-1} - T_n) + m_2 . C_f . (T_{i2} - T_n) + S_n . U_n . (T_a - T_n) \quad (22)$$

All the equations (Eqs. (1) - (22)) were put into SPARK simulation test conditions capable of solving these type of differential equations with a powerful and robust solver [8, 18-19].

3. Experimental setup

There are two different experimental facilities equipped with solar double glazing. The first installation being a test bench consisting of two collectors that can be connected in series or in parallel. The second facility is a complete field of 36 collectors to power the solar cooling installation. In addition, a weather station exists on site to measure solar radiation, air temperature, sky temperature and wind speeds (2 meters and 10 meters above the ground).

*3.1. Design of the solar collector test bench*This test bench consists of two double-glazed flat plate collectors and a storage tank of 300L. The schematic diagram is presented in Fig. 3. To simulate the use of domestic hot water a cooling machine fan coil (5) can be used in order to cool the hot water tank where necessary.

Fig. 3: Test bench schematic: 1. Collector N°1, 2. Collector N°2, 3. Storage tank, 4. Control device, 5. Fan coil.

The objective of the bench work is to test different configurations (in series and in parallel) and study the performance of the solar collectors based on the external operating conditions. This provides a large database to verify the developed dynamic model.

3.2. Solar cooling installation collector field design

Fig. 4: Solar collector field of the solar cooling process

Fig. 4 presents the solar cooling installation double glazing solar collector field. It is composed of 36 collectors divided into 4 branched loops in parallel: 3 loops of 10 collectors in series and 1 loop of 6 collectors. The hot water is stored in the 1500L tank. The hot water feeds an absorption chiller with a cooling power of 30 kW nominal conditions. The cold water is stored in the 1000L cold water tank before being distributed to the 4 teaching classrooms at The University of Reunion [4].

3.3. Uncertainty of the measurements and error analysis

Special attention was paid to the accuracy of the measurements. All temperature sensors installed, both in the test bench and in the 36 solar collectors field are PT100 sensors class A with an accuracy of $\Delta T = \pm 0.15 + 0.002 \cdot T(°C)$ as specified by the manufacturer. This gives high accuracy since the maximum deviation occurred when the temperature reach 100°C is 0.35°C. Solar global radiation is measured using pyranometers with an accuracy of 2%. Before starting the measurements, we compared this pyranometer to another which is installed next to our experimental setup on a weather station. The two pyranometers are installed on the horizontal and the greatest difference noticed between them was 25 W.m^{-2}. Flow meters are used to measure the water flow rates into the collectors. The flow meters have an accuracy of 3%. The capacity recovered by the water is expressed as :

$$Q_{coll} = m_{coll} \cdot c_{p_{water}} \cdot (T_{out} - T_{in}) \quad (23)$$

If the temperature is measured with an uncertainty of ΔT and the water flow rate is measured with the uncertainty of Δm , the relative error committed when measuring the recovered capacity is given by (24)

$$\frac{\Delta Q_{coll}}{Q_{coll}} = \frac{\Delta m_{coll}}{m_{coll}} + \frac{\Delta T_{out} + \Delta T_{in}}{T_{out} - T_{in}}$$

For example, the relative error in the recovered capacity on the 36 solar collectors field when the input temperature is 65°C is estimated to be 9%.

4. Model validation To validate the collector model the simulation results will be compared with results taken from the two experimental installations. The tank model validation will be made with the given data from the solar cooling installation alone. The model data input will be: inlet temperature of the collectors

and flow rate for each component as well as weather conditions on that day (global radiation, wind speed, outside temperature and sky temperature).

4.1. Collector model validation with the test bench

To validate our collector model the calculated outlet temperatures of the 2 collectors taken from the test bench during the simulation and for different configurations, will be compared. In the first case the 2 collectors function in parallel, that is, the same as the input temperature but with 2 different mass flow rates (m_{c1} = 1.23 kg/min for the first collectors et m_{c2} = 1.90 kg/min for the second). The simulations were performed over 2 types of days: global radiation evolution over the two days can be seen in Fig. 5. It can be noted that the first day (day 1) is sunny and the second day (day 2) shows much cloud cover.

Fig. 5: Global solar radiation during the first 2 recorded days

The simulation results as well as a comparison with the experimental data can be seen in Fig 6 and 7. By observing the outlet temperature evolution on the first day (Fig.6) it can be seen that the model follows relatively close to the experimental data for the two collectors.

The absolute error ranges between 0°C and 2.36°C for the first collector and between 0°C et 2.04°C for the second. It can be noted that in both cases the relative error is maximum at the start of the day. The mean absolute errors are 0.76°C for the first case and 0.68°C for the second. The absolute error between the simulated values and measured values, concerning the estimated recuperated energy by the transfer fluid, are 1.31% for the first case and 1.12% for the second over 8 hours in use.

Our model can therefore correctly predict output fluid transfer temperature from the solar collector for high solar radiation days irrespective of the flow chosen. However it is important to study our model performance for days with low solar radiation. Fig. 7 presents output temperature evolution for the second day of the study. It can be pointed out that the model again matches the general aspect of the experimental data each time with a larger deviation at the beginning of the day. The absolute error ranges between 0°C and 3.08°C for the first collector and 0°C and 2.48°C for the second. The mean absolute errors are 0.87°C for the first and 0.68°C for the second. The mean absolute errors at the recuperated energy are 1.34% for the first and 0.84% for the second case.

Fig. 6: Simulated and measured test bench collector outlet temperatures during the first day

Fig. 7: Simulated and measured test bench collector outlet temperatures during the second day

In view of the results, it can be concluded that the model is capable of correctly predicting the solar collector performance regardless of the flow and amplitude of the fluctuations in global radiation throughout the day.The next validation step for the model consists in coupling the two collectors in series and increasing the flow mass (m_{c3} = 2.46 kg/min). Thus the same flow circulates in the 2 collectors; the

temperature of the first collectors output is the same as the input collector temperature of the second. A third experimental day with moderate solar radiation was performed as can be seen in Fig 8. In Fig 9 a comparison between the simulated output temperatures and the two collector's measured temperatures. In the first graph, related to the first collector output temperature, the model again correctly correlates the experimental results with absolute errors ranging from 0°C to 2.19°C and an mean absolute error of 0.52°C. In the second graph representing the second collector output temperature, the model again corresponds relatively well to the experimental results with an absolute error range of 0°C to 2.43°C and a mean absolute error of 0.79°C. The absolute error made for the simulated and measured energy is 1.15% for the first collector and 1.86% for the second over 8 hours of use.

Fig. 8: Solar global radiation during the third recorded day ***Fig. 9: Simulated and measured test bench collector outlet temperatures during the third day***

4.2. Collector model validation with solar cooling collector field The last step in validating the solar collector model consists in modeling the 36 collectors coupling and comparing simulation results with data from our own solar cooling installation. The experimental data was recorded on the same days (day 1 and 2) as for the test bench. The measured output results for the two days can be compared as is seen in Fig. 10.

Fig. 10: Simulated and measured solar collector field outlet temperatures for the 2 recorded days

In Fig. 10 the model again correlates the experimental data for the first day with deviations at the beginning of the day. The absolute error lies between 0°C et 3.57°C for the first day and 0°C et 3.29°C for the second. The mean absolute errors are respectively 0.65°C and 0.74°C and the absolute error for the energy is respectively 3.21% and 1.23%, for the first and second day.

4.3. Stratified tank model validation To validate the stratified tank model a comparison will be made between simulated temperature data taken from the solar cooling installation over 2 functioning days (the same as for the collector field). The input temperatures and the primary and secondary circuit flows; (m_1) and (m_2), were introduced into the model. Fig. 11 depicts changes in primary and secondary flow rates measured over the two days studied. A comparison of these simulated and measured temperatures from the top and bottom of the tank is shown in Fig. 12. Note that in Fig. 11 only the primary circuit pump (m_1) flows into the tank for 1.5 h, where (m_1 = 0.70 kg/s and m_2 = 0 kg/s): this is the tank heating phase. When the tank temperature reaches 80°C, the secondary circuit pump flow starts to feed the absorption chiller (m_1 = 0.70 kg/s et m_2 = 1 kg/s): this is the start of the absorption cycle. Regulation details for solar cooling installation are specified in the article Marc and Al [4].

Fig. 11: Simulated and measured hot tank temperatures over the 2 recorded days ***Fig. 12: Simulated and measured hot tank temperatures over the 2 recorded days***

In Fig. 12 the simulated temperatures from the top and bottom of the tank match those of the experimental values for the two days presented. The absolute errors for the evaluated temperatures at the top of the tank range between 0°C and 2.50°C on the first day and 0°C et 2.10°C on the second. The mean absolute errors are 0.52°C and 0.54°C respectively for the first and second days The errors with relation to the bottom of the tank range between 0°C and 2.30°C for the first day and 0°C and 1.60°C for the second. The mean absolute errors are 0.46°C and 0.30°C respectively for the first and second days.

The mean absolute errors at the primary energy evaluation, are 0.87% and 3.21% respectively for the first and second days. The absolute mean errors for the secondary circuit are 2.70% for the first day and 2.97% for the second day.

In view of the errors it can be concluded that our model is able to take into account thermal stratification in the tank with relatively weak errors when they don't exceed 3.5% for the energy evaluation and 2.5°C for the temperatures. It can be noted that the maximum deviations mainly occur during transitory phases notably at the start of the pump in the secondary loop ($m_2 > 0$).

5. Conclusion This article presents a model for double glazed thermal solar collectors as well as a model for a stratified tank. The model validation phase for the solar collector was divided into 2 parts. In the first part, the simulation results and experimental results from our test bench (2 collectors) were compared. In the second part the solar collector field and stratified tank models from our solar cooling installation at The University Institute of Technology in St Pierre, Reunion Island were presented.Given the calculated absolute errors it can be concluded that our double glazed thermal solar collector model predicts quite well temperature evolutions at the output and therefore energy captured by the transfer fluid whatever the flow rate or magnitude in global radiation fluctuation throughout the day. The maximum absolute error for the output temperature was 3.57°C and the maximum mean error was 0.87°C. The largest deviation mostly occurred at the beginning of the day when the collectors were still cold. The error for the evaluation of the energy recuperated from the transfer fluid was at the most 3.21% which is acceptable in accurately forecasting heat production necessary to feed the absorption chiller of the solar cooling installation. Concerning the simulation results of the stratified tank model, the simulated temperatures at the top and bottom of the tank correctly correlate with the experimental data with absolute errors that attain a maximum of 3.5% for the primary and secondary energy evaluations.

AcknowledgementsThis work has been supported by The French Research National Agency (ANR) through PREBAT 2006 program (ORASOL project).**Appendix A.**

A1 - Values of physical properties for each double glazed solar collector (Eq. 1-19)A2 - Values of physical properties for the hot storage tank (Eq. 20-22)A3 - Summary of calculated absolute errors

Nomenclature

SymbolsC heat capacity [J.kg^{-1}.K^{-1}]e thickness [m]g gravity [m.s^{-2}]
G solar global radiation [W.m^{-2}]
Gr Grashoff number [-]h_{cv} convection exchange coefficient [W.K^{-1}.m^{-2}]h_r radiation exchange coefficient [W.K^{-1}.m^{-2}]k conductive exchange coefficient [W.K^{-1}.m^{-2}]M mass [kg]m mass flow rate [kg.s^{-1}]
Nu Nusselt number [-]
Re Reynolds number [-]S area [m²]T temperature [°C]u velocity [m.s^{-1}]
Greek letters
α absorption coefficient [-]β tilt angle [°]ε emissivity [-]σ Stefan Boltzmann constant [W.K-4.m-2]τ transmission coefficient [-]υ kinematic viscosity [m².s-1]μ dynamic viscosity [kg.s-1.m-1]ρ density [kg.m-3]Λ thermal conductivity [W.K-1.m-1]Subscriptsa1 first air layer a2second air layer
abs absorberamb ambientech exchangerf transfer fluid
g1 first glass collectorg2 second glass collector int insideinf underside ins insulationsup upper side
lat lateral wall

References

1. Ziegler, F., Sorption heat pumping technologies: Comparisons and challenges. International Journal of Refrigeration, 2009. 32(4): p. 566-576.2. Eicker, U. and D. Pietruschka, Design and performance of solar powered absorption cooling systems in office buildings. Energy and Buildings, 2008. 41(1): p. 81-91.3. Mateus, T. and A.C. Oliveira, Energy and economic analysis of an integrated solar absorption cooling and heating system in different building types and climates. Applied Energy, 2008. 86(6): p. 949-957.4. Marc, O., Lucas F., Sinama F., Monceyron E., Experimental investigation of a solar cooling absorption system operating without any backup system under tropical climate. Energy and Buildings, 2010. 42(6): p. 774-782.5. Zambrano, D., Bordons C., Garcia-Gabin W., Camacho E.F., Model development and validation of a solar cooling plant. International Journal of Refrigeration, 2007. 31(2): p. 315-327.6. Atmaca, I. and A. Yigit, Simulation of solar-powered absorption cooling system. Renewable Energy, 2003. 28(8): p. 1277-1293.7. Lecuona, A., Ventas R., Venegas M., Zacarías A., Salgado R., Optimum hot water temperature for absorption solar cooling. Solar Energy, 2009. 83(10): p. 1806-1814.8. Bourdoukan, P., Wurtz E., Joubert P., Spérandio M., Potential of solar heat pipe vacuum collectors in the desiccant cooling process: Modelling and experimental results. Solar Energy, 2008. 82(12): p. 1209-1219.9. Khoukhi, M. and Maruyama S., Theoretical approach of a flat plate solar collector with clear and low-iron glass covers taking into account the spectral absorption and emission within glass covers layer. Renewable Energy, 2004. 30(8): p. 1177-1194.10. Esen, M. and Esen H., Experimental investigation of a two-phase closed thermosyphon solar water heater. Solar Energy, 2005. 79 (5): p. 459-468.

11. Esen, M., Thermal performance of a solar cooker integrated vacuum-tube collector with heat pipes containing different refrigerants. Solar Energy, 2004. 76 (6): p. 751-757.

12. Andersen, E. and Furbo S., Theoretical variations of the thermal performance of different solar collectors and solar combi systems as function of the varying yearly weather conditions in Denmark. Solar Energy, 2009. 83 (4): p.552-565

13. Kumar, R. and Rosen M.A., Thermal performance of integrated collector storage solar water heater with corrugated absorber surface. Applied Thermal Engineering, 2010. 30 (13): p. 1764-1768

14. Agarwal, V.K. and Larson D.C., Calculation of the top loss coefficient of a flat-plate collector. Solar Energy, 1981. 27(1): p. 69-71.15. Duffie, J. and Beckman W., Solar energy thermal processes. New York: Wiley; 1974 [Chapter 4-7]. 1974.16. Incropera, F.P., Dewitt,

D.P., Bergman, T.L., Lavine, A.S., Fundamentals of Heat and Mass Transfer. Book 6th Edition, 2006: p. 514.17. Klein, S.A., A Design Procedure for Solar Heating Systems. Ph.D., University of Wisconsin-Madison. 1976.18. SPARK, Simulation Problem Analysis and Research Kernel. LBNL, California, Berkeley. 2003.19. Sowell, E.F. and Haves P., Efficient solution strategies for building energy system simulation. Energy and Buildings, 2001. 33(4): p. 309-317.

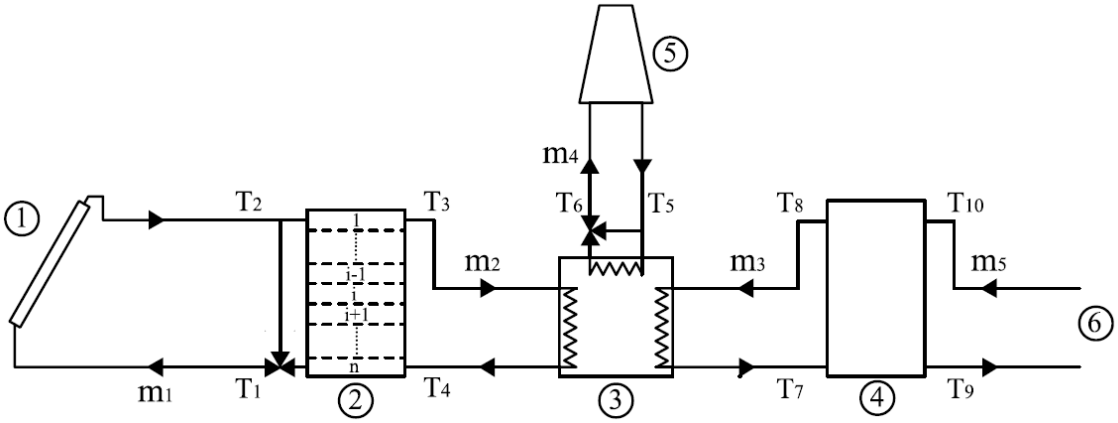

Fig. 1: Diagram of a solar cooling installation: 1. Solar collector field, 2. Hot water tank, 3. Absorption chiller, 4. Cold water tank 5. Cooling tower 6. Building

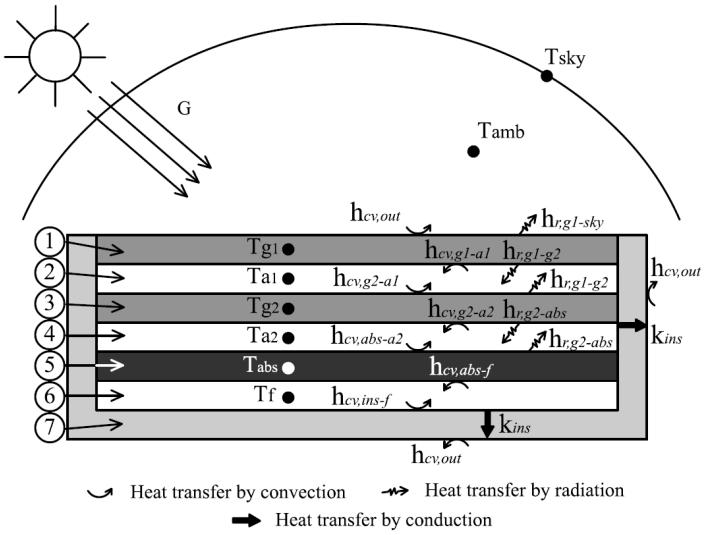

Fig. 2 : Representation of the double glazed collector: 1. First glass layer 2. First air layer 3. Second glass layer 4. Second air layer 5. Absorbent surface 6. Transfer fluid 7. Insulation and support.

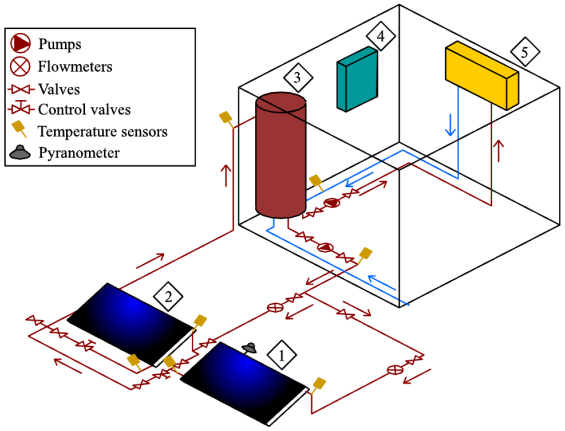

Fig. 3: Test bench schematic: 1. Collector N°1, 2. Collector N°2, 3. Storage tank, 4. Control device, 5. Fan coil.

Fig. 4 : Solar collector field of the solar cooling process

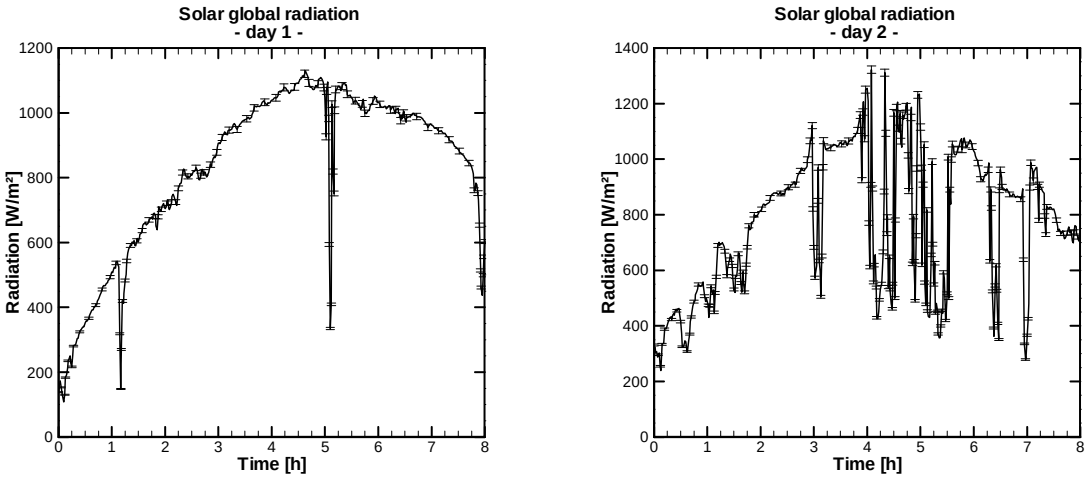

Fig. 5: Global solar radiation during the first 2 recorded days

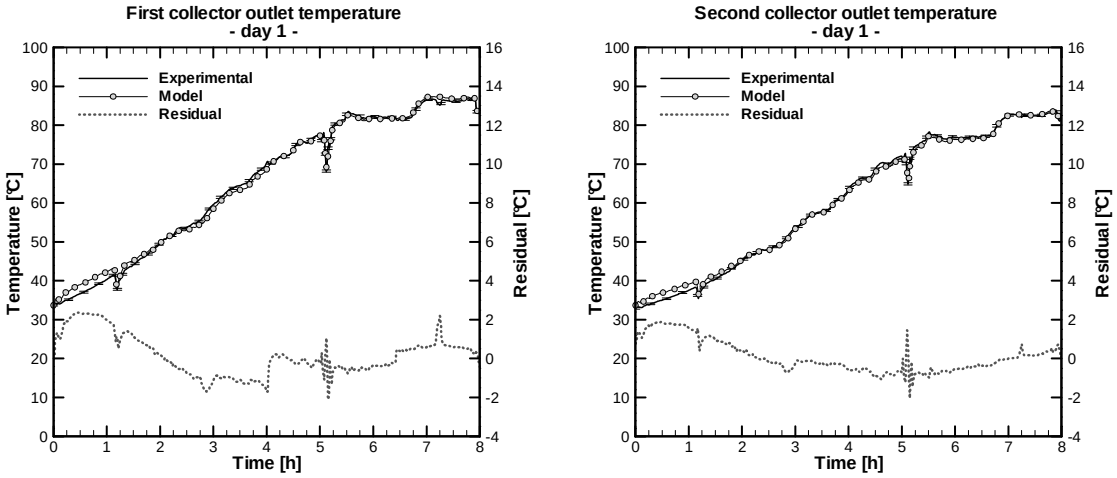

Fig. 6: Simulated and measured test bench collector outlet temperatures during the first day

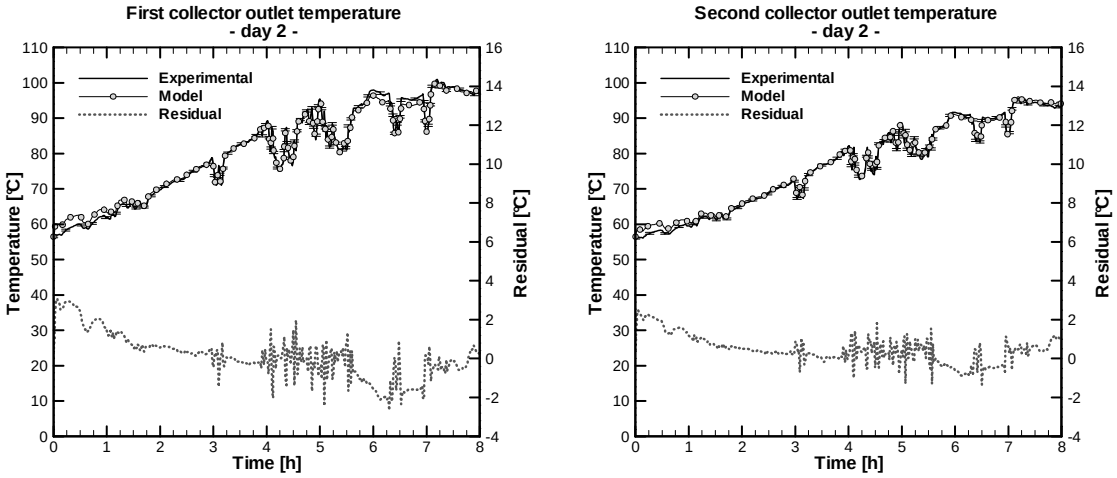

Fig. 7: Simulated and measured test bench collector outlet temperatures during the second day

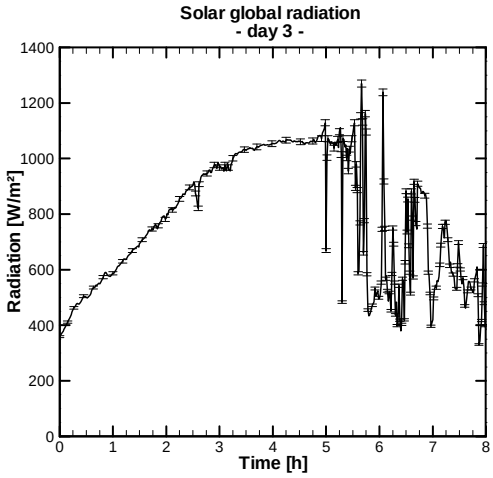

Fig. 8: Solar global radiation during the third recorded day

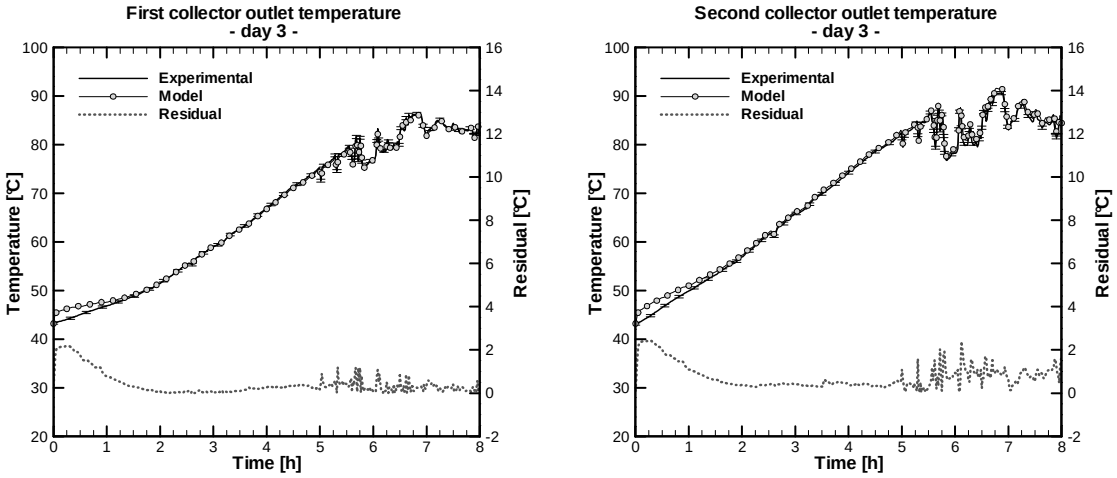

Fig. 9: Simulated and measured test bench collector outlet temperatures during the third day

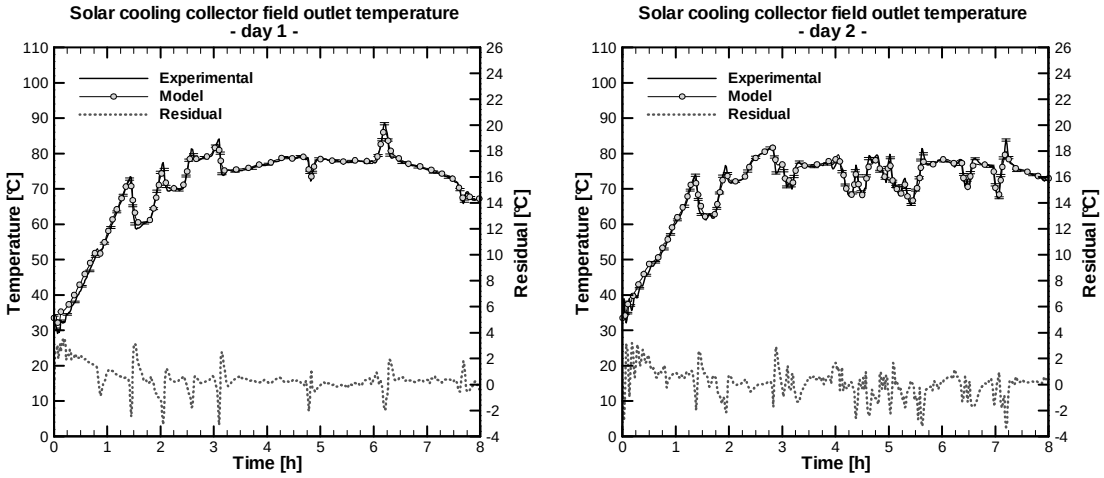

Fig. 10: Simulated and measured solar collector field outlet temperatures for the 2 recorded days

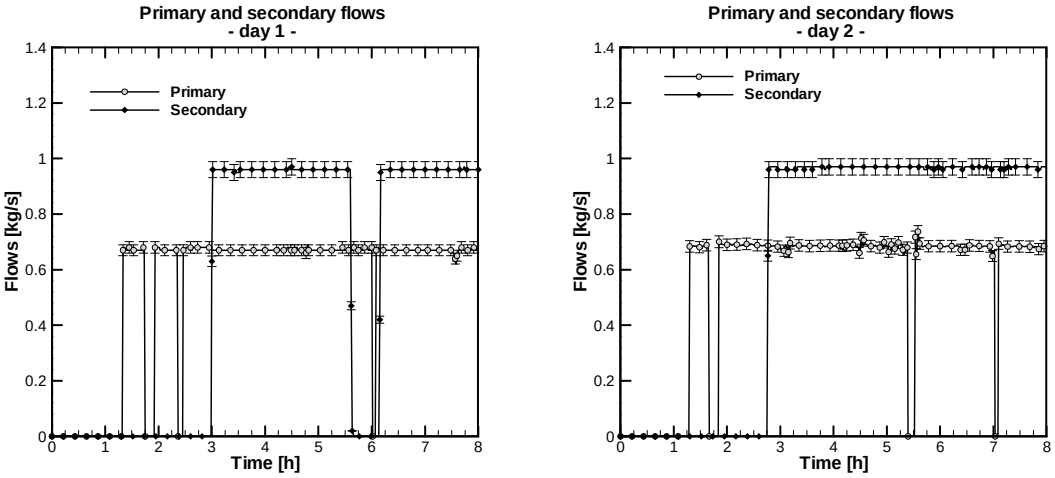

Fig. 11: Simulated and measured hot tank temperatures over the 2 recorded days

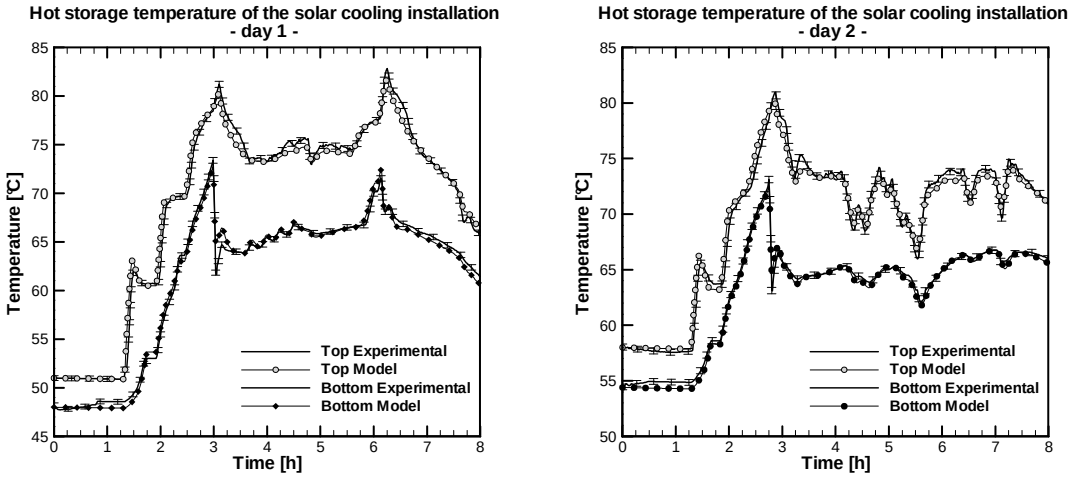

Fig. 12: Simulated and measured hot tank temperatures over the 2 recorded days